Article

Dual Aperture Control on pH- and Anion-Driven Supramolecular Nanoscopic Hybrid Gate-like Ensembles

Rosa Casass, Estela Climent, Ma. Dolores Marcos, Ramn Martnez-Mez, Flix Sancenn, Juan Soto, Pedro Amors, Joan Cano, and Eliseo Ruiz

J. Am. Chem. Soc., **2008**, 130 (6), 1903-1917 • DOI: 10.1021/ja0756772

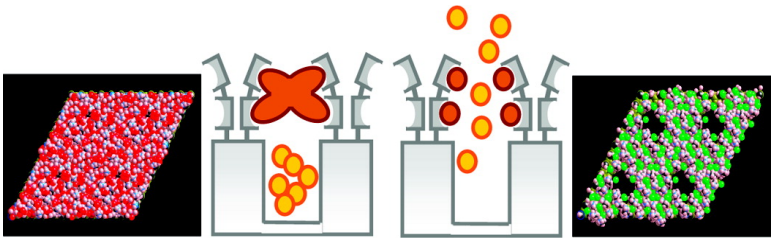

J|A|C|S
ARTICLES
Published on Web 01/23/2008

Dual Aperture Control on pH- and Anion-Driven Supramolecular Nanoscopic Hybrid Gate-like Ensembles

Rosa Casasús,[†] Estela Climent,[†] Mª. Dolores Marcos,[†] Ramón Martínez-Máñez,*[,†] Félix Sancenón,[†] Juan Soto,[†] Pedro Amorós,*[,‡] Joan Cano,*[,§,||] and Eliseo Ruiz[§]

Instituto de Química Molecular Aplicada, Departamento de Química, Universidad Politécnica de Valencia, Camino de Vera s/n, E-46022 Valencia, Spain, Institut de Ciència del Materials, Universitat de València, P.O. Box 22085, E-46071 València, Spain, Departament de Química Inorgànica, Universitat de Barcelona, Diagonal 647, E-08028 Barcelona, Spain, Institut de Química Teòrica i Computacional and Institut de Nanociència i Nanotecnologia, Universitat de Barcelona, E-08028 Barcelona, Spain, and Institució Catalana de Recerca i Estudis Avançats, 08003 Barcelona, Spain

Received August 9, 2007; E-mail: rmaez@qim.upv.es

Ⓦ This paper contains enhanced objects available on the Internet at http://pubs.acs.org/journals/jacsat.

Abstract: The development of gate-like systems able to perform certain programmed functions is an interesting way of taking chemistry to the frontiers of nanoscience. In relation to this field, we report a complete study of the behavior of a pH-driven and anion-controlled nano-supramolecular gate-like ensemble obtained by anchoring suitable polyamines on the pore outlets of mesoporous materials of the type MCM-41 (solid **N3-S**). The release of an entrapped dye ($Ru(bipy)_3^{2+}$) from the pore voids into the bulk solution allows us to study the gating effect. A pH-driven open/close mechanism was observed that arises from the hydrogen-bonding interaction between amines at neutral pH (open gate) and Coulombic repulsions at acidic pH between closely located polyammoniums at the pore openings (closed gate). Molecular dynamics simulations using force field methods have been carried out to explain the pH-driven open/close mechanism. For this purpose, a mesoporous silica structure was constructed, taking as base the $(1\bar{1}1)$ plane of the β-crystoballite structure on which large hexagonal nanopores and anchored polyamines were included. From these calculations, it was observed how completely unprotonated amines display poor coverage of the pore (fully open gate), whereas completely protonated amines (simulating a pH 2 or lower) result in a clear reduction of the pore aperture, in agreement with the experimental results. In additional to the pH-driven protocol, opening/closing of the gate-like ensemble can also be modulated via an anion-controlled mechanism. This study was carried out by monitoring the dye released from the pore voids of the **N3-S** solid at a certain pH in the presence of a range of anions with different structural dimensions and charges, including chloride, sulfate, phosphate, and ATP ($C_{anion} = 1 \times 10^{-2}$ mol dm^{-3}). The choice of a certain anionic guest results in a different gate-like ensemble behavior, ranging from basically no action (chloride) to complete (ATP) or partial pore blockage, depending on the pH (sulfate and phosphate). The remarkable anion-controllable response of the gate-like ensemble can be explained in terms of anion complex formation with the tethered polyamines. These experimental studies are also in agreement with computational simulations with fluoride, chloride, iodide, and dihydrogen phosphate anions. In the model, larger anions push the tethered polyamines toward the pore openings more efficiently, and therefore the pore aperture decreases. The studies also show that, for anions showing a strong tendency to form hydrogen-bonding networks (e.g., phosphate), complete pore blockage was observed at acidic pH. Finally, selectivity patterns have been discussed in terms of kinetic rates of the liberation of the $Ru(bipy)_3^{2+}$ dye from the amine-functionalized dye-containing material **N3-S**.

Introduction

Supramolecular achievements have routinely been arrived at by the stepwise synthesis of molecular architectures via covalent bond formation or by the spontaneous generation of supramolecular forms by self-assembly of simple molecular components in aqueous and nonaqueous solution.[1] One recently suggested alternative to advance new functional aspects in connection with

[†] Universidad Politécnica de València.
[‡] Universitat de València.
[§] Institut de Química Teòrica I Computacional and Institut de Nanociència i Nanotecnologia, Universitat de Barcelona.
[||] Institució Catalana de Recerca i Estudis Avançats.

(1) Lehn, J.-M. *Supramolecular Chemistry: Concepts Perspectives*; VCH: Weinheim, 1995. (b) *Supramolecular Chemistry of Anions*; Bianchi, E., Bowman-James, K., García-España, E., Eds.; Wiley-VCH: New York, 1997.

10.1021/ja0756772 CCC: $40.75

supramolecular ideas is to attach functional molecular entities to pre-organized nanoscopic structures.[2] In recent years there have been important advances in enhanced functional molecular recognition, such as improved signaling on self-assembled monolayers[3] and nanoparticles,[4] switchable host−guest complexation on surfaces,[5] self-assembly structures,[6] molecular machines,[7] etc. Each system involves hybrids that are able to interact and to bind, giving rise to cooperative functional supramolecular behaviors that finally result in chemical amplification processes that would not be found in the unanchored molecule itself. However, most of these examples consist of "flat" 2D surfaces functionalized with certain molecular groups. A step forward, toward additional functional complexity, is the anchoring of molecular entities in 3D nanoscopic scaffolds. Of the prominent examples reported, nanoscopic supramolecular architectures incorporating chemical entities that can act as a supramolecular "gates" are especially attractive. The reported systems are nanoscopic structures functionalized with switchable molecules that can control the state of the gate (closed or open), allowing either the release of the confined guests or the entrance (or access) of molecular species to (or through) certain sites. Broadly speaking, gating properties have been reported on surfaces, in membranes[8] and in porous systems.[9] Of these, we were especially interested in the 3D nanoscopic architectures derived from MCM-41-type siliceous solids. Mesoporous silicas of the MCM-41 family have been paid a lot of attention due to their scientific importance and great potential for applications in a number of research areas.[10] In the field of gated nanochemistry, photochemically, electrochemically, and ionically controlled gate-like elements have been incorporated into 3D MCM-41 scaffolds via tethering molecular or supramolecular gating ensembles on the pore outlets of the mesopores. Thus, in a first "proof-of-concept" paper, Fujiwara et al.[11a,b] reported that they grafted photoresponsive coumarin onto the pore outlets of MCM-41 solids to develop a molecular gate that was photochemically controlled. Irradiation at >350 nm resulted in photodimerization of the coumarin core, which closed the pores by forming a cyclobutane dimer, whereas the gate could be opened by using higher-energy irradiation at 250 nm to regenerate the coumarin monomer by photocleavage of the dimer. Recently, a similar gate-like ensemble was additionally functionalized with a light-driven "molecular stirrer" using the reversible isomerization of azobenzene groups.[11c] The same authors recently reported a redox gate which can be opened and closed by redox-controlled dimerization of thiol groups attached in the pore voids of an MCM-41-type material.[12] Other interesting and remarkable gate-control examples reported by Lin et al. include mesoporous materials containing removable CdS[13] or magnetic nanoparticles.[14] Stoddart and Zink et al. presented supramolecular redox-controlled nanovalves containing grafted pseudorotaxanes and bistable rotaxanes in the pore outlets of mesostructured silica thin films,[15] and recently they reported pH-driven systems containing dialkylammonium threads[16] anchored to MCM-41 and capped with dibenzo[24]crown-8. A pH-responsive gate on mesoporous materials based on a polypseudorotaxane has also been reported by Kim et al.[17] Other pH-driven gate-like elements have been reported by some of the present authors[18a] and by Xiao et al.,[19] in which polyamines or carboxylic acids are anchored on mesoporous silica, respectively. Some of the present authors have also reported a bis-

(2) Descalzo, A. B.; Martínez-Máñez, R.; Sancenón, F.; Hoffmann, K.; Rurack, K. *Angew. Chem., Int. Ed.* **2006**, *45*, 5924−5948.

(3) (a) Zimmerman, R.; Basabe-Desmonts, L.; van der Baan, F.; Reinhoudt, D. N.; Crego-Calama, M. *J. Mater. Chem.* **2005**, *15*, 2772−2777. (b) Basabe-Desmonts, L.; Beld, J.; Zimmerman, R. S.; Hernando, J.; Mela, P.; García Parajó, M. F.; van Hulst, N. F.; van den Berg, A.; Reinhoudt, D. N.; Crego-Calama, M. *J. Am. Chem. Soc.* **2004**, *126*, 7293−7299.

(4) (a) Montalti, M.; Prodi, L.; Zaccheroni, N.; Falini, G. *J. Am. Chem. Soc.* **2002**, *124*, 13540−13546. (b) Montalti, M.; Prodi, L.; Zaccheroni, N. *J. Mater. Chem.* **2005**, *15*, 2810−2814. (c) Brasola, E.; Mancin, F.; Rampazzo, E.; Tecilla, P.; Tonellato, U. *Chem. Commun.* **2002**, 3026−3027. (d) Rampazzo, E.; Brasola, E.; Marcuz, S.; Mancin, F.; Tecilla, P.; Tonellato, U. *J. Mater. Chem.* **2005**, *15*, 2687−2696.

(5) (a) Cooke, G. *Angew. Chem., Int. Ed.* **2003**, *42*, 4860−4870. (b) Corbellini, F.; Mulder, A.; Sartori, A.; Ludden, M. J. W.; Casnati, A.; Ungaro, R.; Huskens, J.; Crego-Calama, M.; Reinhoudt, D. N. *J. Am. Chem. Soc.* **2004**, *126*, 17050−17058. (c) Crespo-Biel, O.; Dordi, B.; Reinhoudt, D. N.; Huskens, J. *J. Am. Chem. Soc.* **2005**, *127*, 7594−7600. (d) Wanunu, M.; Popovitz-Biro, R.; Cohen, H.; Vaskevich, A.; Rubinstein, I. *J. Am. Chem. Soc.* **2005**, *127*, 9207−9215. (e) Morisue, M.; Yamatsu, S.; Haruta, N.; Kobuke, Y. *Chem. Eur. J.* **2005**, *11*, 5563−5574. (f) Onelin, S.; Huskens, J.; Ravoo, B. J.; Reinhoudt, D. N. *Small* **2005**, *1*, 852−857. (g) Banerjee, I. A.; Yu, L.; Matsui, H. *J. Am. Chem. Soc.* **2003**, *125*, 9542−9543. (h) Chen, Y.-F.; Banerjee, I. A.; Yu, L.; Djalali, R.; Matsui, H. *Langmuir* **2004**, *20*, 8409−8413.

(6) (a) Reinhoudt, D. N.; Crego-Calama, M. *Science* **2002**, *295*, 2403−2407. (b) Liu, J.; Alvarez, J.; Ong, W.; Kaifer, A. E. *Nano Lett.* **2001**, *1*, 57−60. (c) Liu, Y.; Wang, H.; Chen, Y.; Ke, C. F.; Liu, M. *J. Am. Chem. Soc.* **2005**, *127*, 657−666. (d) Crespo-Biel, O.; Jukovic, A.; Karlsson, M.; Reinhoudt, D. N.; Huskens, J. *Isr. J. Chem.* **2005**, *45*, 353−362. (e) Mulder, A.; Huskens, J.; Reinhoudt, D. N. *Org. Biomol. Chem.* **2004**, *2*, 3409−3424. (f) Naka, K.; Roh, H.; Chujo, Y. *Lamgmuir* **2003**, *19*, 5496−5501.

(7) (a) Kay, E. R.; Leigh, D. A.; Zerbetto, F. *Angew. Chem., Int. Ed.* **2007**, *46*, 72−191. (b) Balzani, V.; Credi, A.; Silvi, S.; Venturi, M. *Chem. Soc. Rev.* **2005**, *35*, 1135−1149. (c) Collin, J.-P.: Heitz, V.; Sauvage, J.-P. *Top. Curr. Chem.* **2005**, *262*, 29−62. (d) Kay, E. R.; Leigh, D. A. *Top. Curr. Chem.* **2005**, *262*, 133−177. (e) Hernandez, J. V.; Kay, E. R.; Leigh, D. A. *Science* **2004**, *306*, 1532−1537. (f) Flood, A. H.; Ramirez, R. J. A.; Deng, W.-Q.; Muller, R. P.; Goddard, W. A.; Stoddart, J. F. *Aust. J. Chem.* **2004**, *57*, 301−322. (g) van Delden, R. A.; ter Wiel, M. K. J.; De Jong, H.; Meetsma, A.; Feringa, B. L. *Org. Biomol. Chem.* **2004**, *2*, 1531−1541. (h) Dietrich-Buchecker, C.; Jiménez-Molero, M. C.; Sartor, V.; Sauvage, J. P. *Pure Appl. Chem.* **2003**, *75*, 1383−1393. (i) Barboiu, M.; Lehn, J.-M. *Proc. Natl. Acad. Sci. U.S.A.* **2002**, *99*, 5201−5206. (j) Balzani, V.; Credi, A.; Raymo, F.; Stoddart, J. F. *Angew. Chem., Int. Ed.* **2000**, *39*, 3348−3391.

(8) See, for instance: (a) Jung, Y.; Bayley, H.; Movileanu, L. *J. Am. Chem. Soc.* **2006**, *128*, 15332−15340. (b) Joseph, S.; Mashl, R. J.; Jakobsson, E.; Aluru, N. R. *Nano Lett.* **2003**, *3*, 1399. (c) Jeong, B.; Gutowska, A. *Trends Biotechnol.* **2002**, *20*, 305−311. (d) Rusell, T. P. *Science* **2002**, *297*, 964−967. (e) Ding, Z. L.; Fong, R. B.; Long, C. J.; Stayton, P. S.; Hoffman, A. S. *Nature* **2001**, *411*, 59−62. (f) Galaev, I. Y.; Mattiasson, B. *Trends Biotechnol.* **1999**, *17*, 335−340. (g) Okano, T.; Bae, Y. H.; Jacobs, H.; Kim, S. W. *J. Controlled Release* **1990**, *11*, 255. (h) Sugawara, M.; Kojima, K.; Sazawa, H.; Umezawa, Y. *Anal. Chem.* **1987**, *59*, 2842.

(9) Of special relevance is the development of artificial channels. See, for instance: (a) Yamaguchi, T.; Ito, T.; Sato, T.; Sginbo, T.; Nakao, S. *J. Am. Chem. Soc.* **1999**, *121*, 4078. (b) Berger, J.; Reist, M.; Mayer, J. M.; Felt, O.; Peppas, N. A.; Gurny, R. *Eur. J. Pharm. Biopharm.* **2004**, *57*, 19.

(10) (a) Kesge, C. T.; Leonowicz, M. E.; Roth, W. J.; Vartuli, J. C.; Beck, J. S. *Nature* **1992**, *359*, 710. (b) Zhao, D.; Feng, J.; Huo, Q.; Melosh, N.; Fredrickson, G. H.; Chmelka, B. F.; Stucky, G. D. *Science* **1998**, *279*, 548. (c) Liu, Y.; Zhang, W.; Pinnavaia, T. J. *Angew. Chem., Int. Ed.* **2001**, *40*, 1255. (d) Han, Y.; Li, D.; Zhao, L.; Xiao, F.-S. *Angew. Chem., Int. Ed.* **2003**, *42*, 3633.

(11) (a) Mal, N. K.; Fujiwara, M.; Tanaka, Y. *Nature* **2003**, *421*, 350−353. (b) Mal, N. K.; Fujiwara, M.; Tanaka, Y.; Taguchi, T.; Matsukata, M. *Chem. Mater.* **2003**, *15*, 2285−3394. (c) Zhu, Y.; Fujiwara, M. *Angew. Chem., Int. Ed.* **2007**, *46*, 2241−2244.

(12) Fujiwara, M.; Terashima, S.; Endo, Y.; Shiokawa, K.; Ohue, H. *Chem. Commun.* **2006**, 4635−4637.

(13) Lai, C.-Y.; Trewyn, B. G.; Jeftinija, D. M.; Jeftinija, K.; Xu, S.; Jeftinija, S.; Lin, V. S.-Y. *J. Am. Chem. Soc.* **2003**, *125*, 4451−4459.

(14) Giri, S.; Trewyn, B. G.; Stellmaker, M. P.; Lin, V. S.-Y. *Angew. Chem., Int. Ed.* **2005**, *44*, 5038−5044.

(15) (a) Hernandez, R.; Tseng, H.-R.; Wong, J. W.; Stoddart, J. F.; Zink, J. I. *J. Am. Chem. Soc.* **2004**, *126*, 3370−3371. (b) Nguyen, T. D.; Tseng, H.-R.; Celeste, P. C.; Flood, A. H.; Liu, Y.; Stoddart, J. F.; Zink, J. I. *Proc. Natl. Acad. Sci. U.S.A.* **2005**, *102*, 10029−10034. (c) Nguyen, T. D.; Liu, Y.; Saha, S.; Leung, K. C.-F.; Stoddart, J. F.; Zink, J. I. *J. Am. Chem. Soc.* **2007**, *129*, 626−634.

(16) Nguyen, T. D.; Leung, K. C-F.; Liong, M.; Pentecost, C. D.; Stoddart, J. F.; Zink, J. I. *Org. Lett.* **2006**, *8*, 3363−3366.

(17) Park, C.; Oh, K.; Lee, S. C.; Kim, C. *Angew. Chem., Int. Ed.* **2007**, *46*, 1455−1457.

(18) (a) Casasús, R.; Marcos, M. D.; Martínez-Máñez, R.; Ros-Lis, J. V.; Soto, J.; Villaescusa, LA.; Amorós, P.; Beltrán, D.; Guillem, C.; Latorre, J. *J. Am. Chem. Soc.* **2004**, *126*, 8612−8613. (b) Aznar, E.; Casasús, R.; García-Acosta, B.; Marcos, M. D.; Martínez-Máñez, R.; Sancenón, F.; Soto, J.; Amorós, P. *Adv. Matter.* **2007**, *19*, 2228−2231.

(19) Yang, Q.; Wang, S.; Fan, P.; Wang, L.; Di, Y.; Lin, K.; Xiao, F.-S. *Chem. Mater.* **2005**, *17*, 5999−6003.

Scheme 1. Molecular Gate Controlled by Coordination of Target Anions with Certain Binding Sites

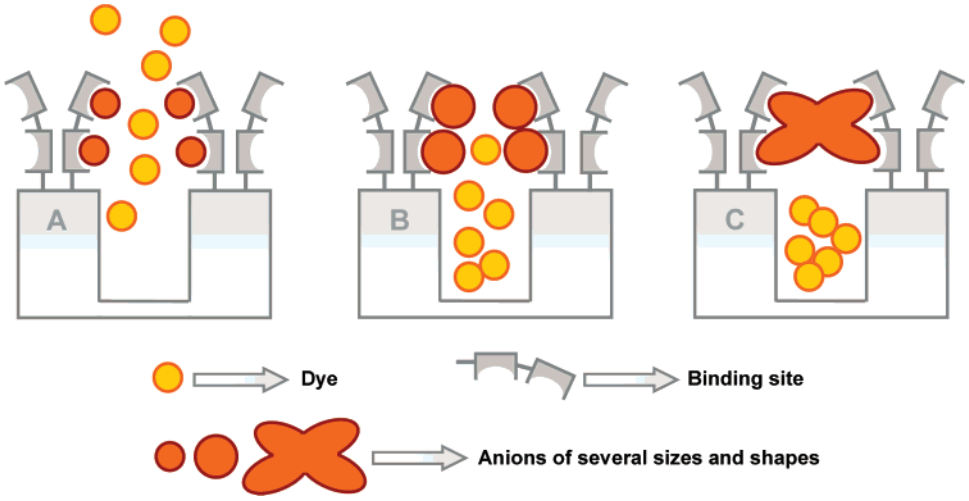

switching gate-like system controllable by light and chemical inputs using spiropyran moieties and carboxylate-containing dendrimers.[18b] Relevant examples on the regulation of the pore size in mesoporous systems have also been reported, using photoresponsive azobenzene-modified pore surfaces[20] or cleavable tails of suitable templates placed on the pore voids.[21] Most of these systems are designed for delivery assays and, less commonly, for sensing protocols.[22] Interesting examples containing gate-like systems have also been reported in which nanotubes are used as suitable containers.[23]

Despite the novelty of these examples, they still often harbor disadvantages for their potential use in advanced applications. From the literature, it is apparent that examples of gate-like ensembles that operate reversibly in response to multiple-channel stimuli and that are able to execute gate-like behavior in aqueous solution are still rare. The development of gate-like systems able to perform certain programmed functions would be an interesting way to take chemistry to the frontiers of nanoscience. In relation to this field, we believe that the functionalization of 3D mesoporous scaffolds with suitable molecular entities capable of displaying "classical" coordination behavior is a promising starting point for applying the versatility of supramolecular ideas to the design of nanoscopic devices, such as gate-like systems, and a way of studying the factors that could influence the design of molecular gating functions based on hetero-supramolecular concepts.

The design of coordination-controlled gate-like ensembles is depicted in Scheme 1 and consists of the use of a suitable mesoporous support containing pores loaded with a certain molecule (for instance, a dye) and binding sites of different natures grafted on the pore outlets. The coordinative behavior of the binding sites with guests of varying natures would determine the kinetic release of the dye from the pores and eventually close the gate. As exemplified in Scheme 1, guests of different sizes (A and B), shapes (C), or charges (not shown) would provide precise control of the release of the entrapped molecular entity.

This article deals with a subject that we find particularly captivating: the supramolecular functional aspects that arise from the covalent grafting of organic molecules to pre-organized or pre-existing stable nanoscopic supports. In particular, we report here on the design of a nanoscopic molecular movable gate-like functional hybrid system that can be controlled by both the pH and the presence of certain anions. For this purpose, the nanoscopic MCM-41-based material was synthesized and grafted onto the pore outlets with polyamines of different sizes. The gating effect is studied via storage and controlled release of a dye (the $[Ru(bipy)_3]^{2+}$ complex) from the pore voids through the gate-like ensemble to the bulk solution. In order to analyze the factors that open or close the gate, we carried out calculations of release kinetics. Finally, geometry optimizations and molecular dynamics simulations using force-field methods are presented in order to analyze the dual pH- and anion-driven gate-like mechanism.

Results and Discussion

Design Considerations. The development of responsive nanoscopic molecular gates requires the choice of two components: (i) suitable "gate-like ensembles" able to change one or several properties (size, shape, bulkiness, etc.) upon external stimuli and (ii) the selection of a nanostructured matrix onto which the gate-like scaffold is grafted. For the latter, we chose mesoporous materials of the MCM-41 family as a suitable inorganic matrix, due to its high homogeneous porosity, inertness, and ease of functionalization on the external (or internal) surface.[24] Also, the presence of pores with a diameter of ca. 2−3 nm allows for a rapid uptake and release of selected guests, while allowing supramolecular (vide infra) coordinative effects to be studied on the nanometric scale. In relation to the first component, the gate-like ensemble, it was our aim to

(20) Liu, N.; Dunphy, D.; Atanassov, P.; Bunge, S. D.; Chen, Z.; López, G. P.; Boyle, T. J.; Brinker, C. J. *Nano Lett.* **2004**, *4*, 551−554.
(21) Zhang, Q.; Ariga, K.; Okabe, A.; Aida, T. *J. Am. Chem. Soc*. **2004**, *126*, 988−989.
(22) (a) Casasús, R.; Aznar, E.; Marcos, M. D.; Martínez-Máñez, R.; Sancenón, F.; Soto, J.; Amorós, P. *Angew. Chem., Int. Ed.* **2006**, *45*, 6661−6664. (b) Coll, C.; Casasús, R.; Aznar, E.; Marcos, M. D.; Martínez-Máñez, R.; Sancenón, F.; Soto, J.; Amorós, P. *Chem. Commun*. **2007**, 1957−1959.
(23) (a) Nednoor, P.; Chopra, N.; Gavalas, V.; Bachas, L. G.; Hinds, B. J. *Chem. Mater*. **2005**, *17*, 3595−3599. (b) Hillebrenner, H.; Buyukserin, F.; Kang, M.; Mota, M. O.; Stewart, J. D.; Martin, C. R. *J. Am. Chem. Soc*. **2006**, *128*, 4236−4237.
(24) (a) Beck, J. S.; Vartuli, J. C.; Roth, W. J.; Leonowicz, M. E.; Kresge, C. T.; Schmitt, K. D.; Chu, C. T.-W.; Olson, D. H.; Sheppard, E. W.; McCullen, S. B.; Higgins, J. B.; Schlenker, J. L. *J. Am. Chem. Soc.* **1992**, *114*, 10834−10843. (b) Wright, A. P.; Davis, M. E. *Chem. Rev.* **2002**, *102*, 3589−3614. (c) Kickelbick, G. *Angew. Chem., Int. Ed.* **2004**, *43*, 3102−3104. (d) Stein, A. *Adv. Mater*. **2003**, *15*, 763−775.

Scheme 2. Illustration of the Synthetic Procedure for the Preparation of the Solids **N3-S** and **N1-S**[a]

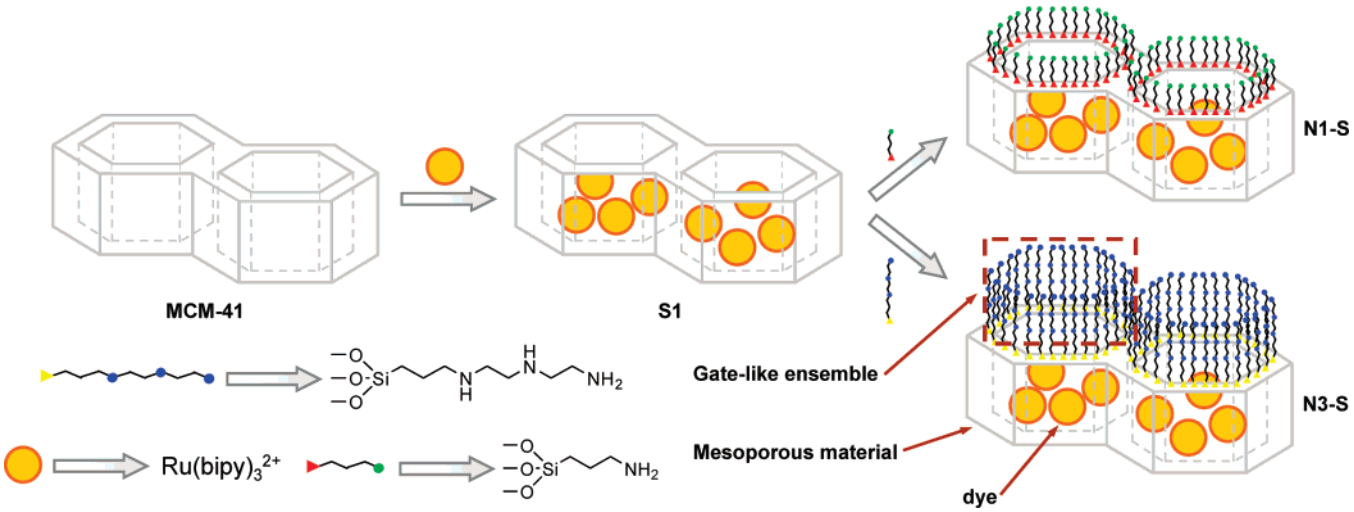

[a] In the first step, the pores of the mesoporous MCM-41 material are loaded with the $[Ru(bipy)_3]^{2+}$ dye to give **S1**, which was further reacted with 3-[2-(2-aminoethylamino)ethylamino]propyl-trimethoxysilane or 3-aminopropyl-trimethoxysilane to obtain **N3-S** and **N1-S**, respectively, followed by washing to remove the excess of substrates. The prepared solids are ready to be used in dye-releasing studies in water.

develop a gate platform that could operate in aqueous solution and could be triggered by simple external stimuli such as pH changes or well-known coordination events. For this purpose, we selected polyamines. Polyamines are well-known pH-responsive molecules that can additionally complex anions via electrostatic forces and by formation of hydrogen-bonding interactions in a wide pH range. From the various possibilities, we selected the derivatives 3-[2-(2-aminoethylamino)ethylamino]propyl-trimethoxysilane and 3-aminopropyl-trimethoxysilane as simple, but suitable, open-chain molecular entities that were anchored through covalent bonds on the pore outlets of an MCM-41 material. The functional open/close protocol of the nanoscopic gate-like ensemble was tested by measuring the release of a dye ($[Ru(bipy)_3]Cl_2$, where bipy = 2,2′-bipyridine) loaded on the inner mesopores of the 3D organized MCM-41 solid. The ruthenium(II) complex was chosen because of its relatively high molar absorptivity and its high solubility and stability in water in a wide pH range. The gate-like effect can then be straightforwardly studied via the delivery of the dye from the pore voids to the aqueous solution through monitorization, in the water phase, of the spin-allowed d−π metal-to-ligand charge-transfer transition band of the $Ru(bipy)_3^{2+}$ complex centered at 454 nm.

In the synthesis of the gating material, the inorganic 3D matrix, dye, and amine groups should be arranged in a programmed fashion. Thus, the solid matrix (MCM-41-type solids) must contain the dye (the delivered molecule) in the pores, whereas the molecular movable mechanism (the amine-based gate-like ensemble) should ideally only be anchored on the outer surface (the pore outlets). To prepare this organized hybrid material (see Scheme 2), we first synthesized the mesoporous scaffold using tetraethyl orthosilicate (TEOS) as hydrolytic inorganic precursor and the surfactant hexadecyl-trimethylammonium bromide (CTAB) as porogen species. Calcination of the mesostructured phase resulted in the starting solid, MCM-41. After removal of adsorbed water by azeotropic distillation, the dye tris(2,2′-bipyridyl)ruthenium(II) chloride was added to the suspension and stirred for 24 h with the aim of completely loading the pores of the MCM-41 scaffolding. After this, an excess of 3-[2-(2-aminoethylamino)ethylamino]propyl-trimethoxysilane (to yield **N3-S**) or 3-aminopropyl-trimethoxysilane (to yield **N1-S**) was added and the suspension stirred. The amine−silane derivative is added to the suspension that still contains a high concentration of the dye in order to disfavor the diffusion of the latter from the pores out to the solution. The final orange solids (**N3-S** and **N1-S**) were filtered, washed with acetonitrile, and dried at 70 °C for 12 h. This method, loading of the mesopores followed by grafting of the gate-like ensemble, would result in a final solid basically containing dyes in the interior of the mesopore and the gate-like ensemble shaped on the outside of the pores. In fact, a similar two-step synthetic procedure has been used recently by other authors to develop similar responsive operational gating structures.[13,14,16,17] Thus, although it cannot be completely ruled out that some organosilane molecules could diffuse into the mesopores at the same time that some dye molecules can diffuse out during the second step, the accepted quick anchoring of the organosilane (typically some few minutes) and the expected relatively slow diffusion of the dye make it feasible to obtain gate-like structures such as that schematically shown in Scheme 2. The final solids were characterized by elemental analysis, thermogravimetric analysis (TGA), porosimetry, and powder X-ray diffraction (PXRD).

A schematic representation of the hybrid functionalized **N1-S** and **N3-S** solids is shown in Scheme 2. It is apparent that only the tethered amines which are gathered around the pore outlets will be related with the functional gating effect observed (see below), whereas other amines anchored far from the pore openings (not shown in the scheme) will exert a much smaller effect on the gating mechanism. The following discussions will therefore be focused on this particular nanoscopic superstructure that will be known as the "gate-like ensemble". For the sake of comparison, the control hybrid solid **N3-SF** was also prepared. This consisted of a silica fumed matrix (having a 2D surface) that was reacted with 3-[2-(2-aminoethylamino)ethylamino]-propyl-trimethoxysilane and also contained a certain amount of adsorbed $Ru(bipy)_3^{2+}$ dye.

Characterization of the Hybrid Materials. Figure 1 shows powder X-ray patterns of the solids MCM-41 as-synthesized, MCM-41 calcined, and the final **N3-S** and **N1-S** solids containing the dye and the anchored amines. The PXRD of siliceous

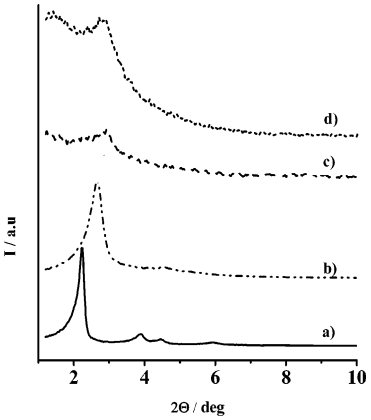

Figure 1. Powder X-ray patterns of the solids (a) MCM-41 as-synthesized, (b) MCM-41 calcined, and the final (c) **N3-S** and (d) **N1-S** containing the dye and the anchored amines.

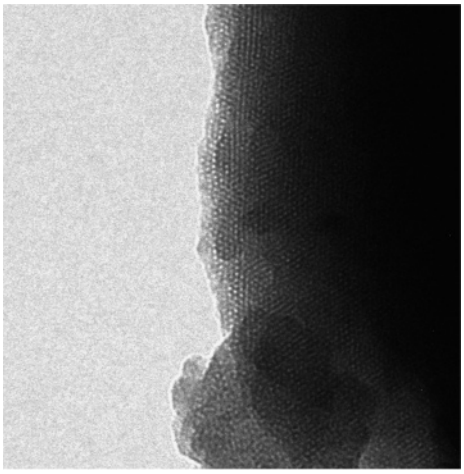

Figure 2. TEM image of the solid **N3-S** showing the typical disordered hexagonal porosity of the MCM-41 matrix.

MCM-41 as-synthesized shows four low-angle reflections typical of a hexagonal array that can be indexed as (100), (110), (200), and (210) Bragg peaks with an a_0 cell parameter of 45.6 Å (d_{100} spacing of 39.5 Å). A significant displacement of the (100) peak in the XRD powder of the MCM-41 calcined sample is clearly appreciated in the curve b, corresponding to an approximate cell contraction of 7 Å. This displacement and the broadening of the (110) and (200) peaks are related to further condensation of silanols during the calcination step. In Figure 1, curves c and d correspond to the **N3-S** and **N1-S** XRD patterns. In this case, the loss of the (110) and (200) reflections is observed, most likely related to a loss of contrast due to the filling of the pore voids with the ruthenium(II) dye. Nevertheless, the value and intensity of the d_{100} peak in this pattern strongly evidences that the loading process with the dye and the further functionalization with amine groups have not damaged the mesoporous 3D MCM-41 scaffolding. The presence in the final functionalized solids of the mesoporous structure is also observed from the TEM analysis, in which the typical disordered hexagonal porosity of the MCM-41 matrix can be seen (see Figure 2).

In relation to the N_2 adsorption−desorption isotherms, the MCM-41 calcined solid shows typical curves for this class of material, consisting of one single adsorption step at the intermediate P/P_0 value (see Figure 3). This curve corresponds to a type IV isotherm, in which the process observed can be

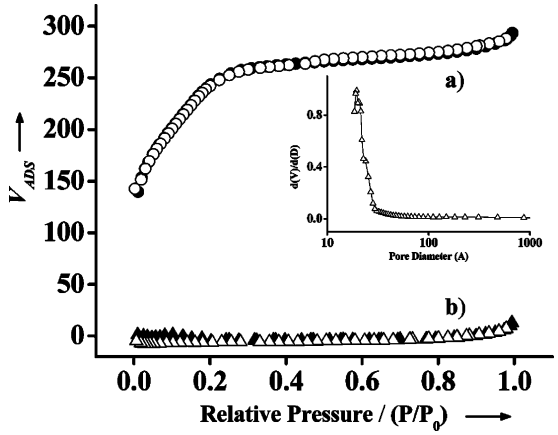

Figure 3. Nitrogen adsorption−desorption isotherms for (a) the **MCM-41** mesoporous material and (b) the dye-loaded and amine-functionalized **N3-S** material. V_{ADS} is the volume adsorbed (cm^3/g). Inset: Pore size distribution for **MCM-41** material.

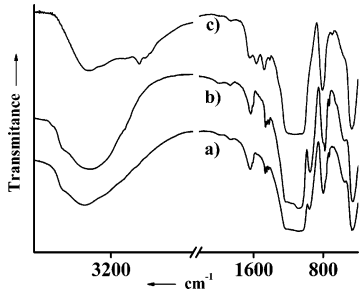

Figure 4. Infrared spectra of solids (a) **N3-S**, (b) **S1**, and (c) **N3-SF**.

related to the nitrogen condensation inside the mesopores by capillarity. The absence of a hysteresis loop in this interval and the narrow pore distribution suggest the existence of uniform cylindrical mesopores (2.05 nm, 0.35 $cm^3\ g^{-1}$; inset in Figure 3). Application of the BET model gave a value for the total specific surface of 893 $m^2\ g^{-1}$. Figure 3 also shows (curve b) the isothermal nitrogen adsorption−desorption behavior of the **N3-S** material. The flat curves obtained for this functionalized hybrid solid indicate the absence of any porosity and, together with the preservation of the pseudo-hexagonal ordering deduced from the PXRD and the TEM images, provide direct evidence of the high efficiency of the dye loading. On the other hand, the **N3-S** derivative, after complete dye delivery, displays adsorption−desorption isotherms showing an appreciable increase of ca. 400 m^2/g in BET surface area when compared to the full-dye loaded solid. This fact supports the inclusion of the dye inside the mesopores.

Infrared spectroscopy is also a suitable technique for following functionalization from the starting MCM-41 solid. Figure 4 shows the infrared spectra of **S1** and **N3-S**, as well as the IR spectrum of the **N3-SF** solid. The dominant bands are those due to the silica matrix (1250, 1087, and 802 cm^{-1}) and those related to the vibrations of water molecules (3420 and 1620 cm^{-1}). Regarding the dye loading and functionalization process, small bands related to the organic moieties (bipyridine and propyldiethylenetriamine or propylamine) can also be observed. The presence of amine groups was confirmed with the δ_{NH} transitions at 3150 and 1573−1430 cm^{-1}, corresponding to N−H vibrations. In the case of the **N3-SF** material, bands related to the C−H stretching vibrations at 2900 cm^{-1} are also observed. Another important feature is the drop in intensity of the band

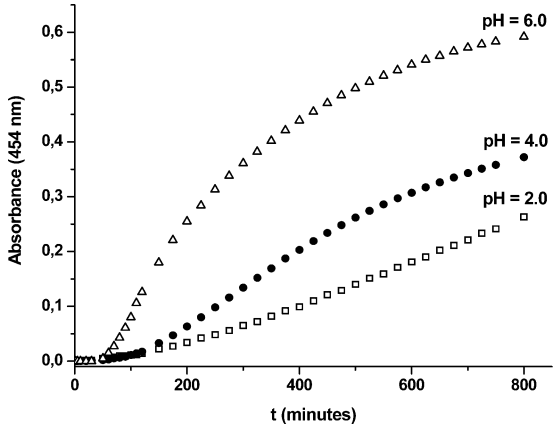

Figure 5. Release profiles of the ruthenium(II) complex from the pores of solid **N3-S** at pH 2, 4, and 6 in the presence of chloride.

Table 1. Dye and Polyamine Content of **N3-S**, **N1-S**, and **N3-SF** Materials Obtained from Thermogravimetric and CHN Elemental Analyses

sample	$[Ru(bipy)_3]^{2+}$:Si (mol:mol)	amine:Si (mol:mol)
N3-S	0.014	0.031
N1-S	0.021	0.027
N3-SF	0.007	0.066

at 952 cm^{-1}, related to the vibration of the silanol groups for the amine-functionalized materials.

Quantification of the content of the amine groups and the $Ru(bipy)_3^{2+}$ dye was accomplished by thermogravimetric studies and elemental and enegry-dispersive X-ray (EDX) analysis. Typical dye and amine contents in the final solids **N3-S**, **N1-S**, and **N3-SF** are shown in Table 1.

Functional pH-Driven Gate-like Ensemble. The effectiveness of the gate-like ensemble with changes in the proton concentration (pH-driven nanogates) was first studied with the hybrid material **N3-S**. With this aim, a range of pH values was employed to effect the controlled release of the ruthenium(II) complex from the pore voids into the aqueous solution. For the sake of clarity, we will detail herein the results obtained at three different pH values (2, 4, and 6), at which differentiable behavior was observed. Basic pH values were avoided in the study in order to prevent the possible serious degradation of the siliceous matrix. In a typical dye-release experiment, 10 mg of **N3-S** was placed in a plastic cartridge, and then water at a certain pH was passed through the sample for 800 min. The increase in the absorption band at 454 nm in the aqueous solution indicated a corresponding leaking out of the $Ru(bipy)_3^{2+}$ complex from the pores. The pH-controllable gating effect can be seen in Figure 5, which plots the release profiles of the ruthenium(II) complex for solid **N3-S** at pH 2, 4, and 6. In order to study only the effect of the pH on the operation of the gate-like ensemble (see below for a anion-controllable functional effect), the proton concentration was adjusted in all cases with hydrochloric acid, and in all the experiments the final concentration of the chloride anion was fixed at 0.01 mol dm^{-3} (completed in each case by adding the corresponding amount of sodium chloride). Figure 5 shows that the dye delivery is relatively low at pH 2, compared to that at pH 6, where there is considerable leakage of the ruthenium complex; i.e., the gate-like ensemble is fully open. At an intermediate pH (pH 4), the gate-like ensemble is ajar. The interpretation of such behavior is to be found in the different degrees of protonation of the amines in the pore voids. Thus, although both the pH-driven and anion-driven (vide infra) mechanisms are closely interconnected and it is not easy to weigh their individual contributions (i.e., acidification necessarily includes protonation of the amines and therefore interaction between the polyammonium groups and the corresponding anion), we believe that there is a pH-driven open/close mechanism that arises from the hydrogen-bonding interaction between amines at neutral pH (open gate) and Coulombic repulsions at acidic pH between closely located polyammoniums at the pore openings (closed gate). When protonated, the tethered open-chain polyamines in the gate-like ensemble tend to adopt a rigid-like conformation that will push them away to the pore openings. This results in a pore blockage that inhibits (complete or partially) the release of the ruthenium(II) complex. This basic pH-driven mechanism is supported by molecular modeling calculations (see below) and is schematically shown in Scheme 3.

Scheme 3. Schematic Representation of the Functional pH-Controlled Gating Mechanism

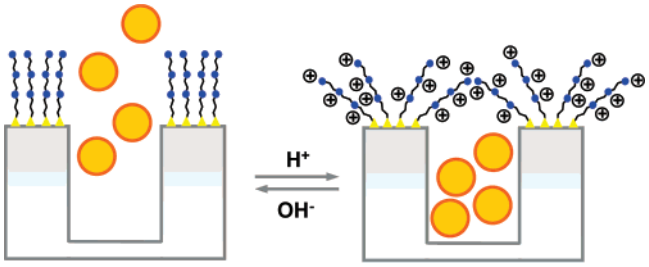

This pH effect is dependent on the degree of protonation. A triamine similar to that anchored in the **N3-S** solid, such as diethylentriamine ($H_2N-CH_2-CH_2-NH-CH_2-CH_2-NH_2$), has p$K_a$ values in water of 9.84, 9.02, and 4.23.[25] However, it has to be taken into account that these pK_a values are expected to be significantly modified when a number of polyamines are anchored to the silica surface. To understand the different behavior, it is necessary to be aware that pK_a values in linear polyamines can easily be rationalized bearing in mind simple electrostatic considerations. Prediction models are based on the concept that it is more difficult to protonate amines placed close to an already protonated ammonium group; therefore, in polyamines, the stepwise pK_a values decrease as the number of protonated amines increases.[26] Thus, although the pK_a values of aliphatic amines (monoamines) are typically around ca. 9−10, in polyamines there are usually as many stepwise constants as number of amine groups; i.e., the amines behave from very basic (first protonations) to poorly basic (last protonations). Thus, a monolayer of amines such as we have in **N3-S** would behave as having a very wide range of pK_a values. Nevertheless, although it is not possible to determine the pK_a of all the individual tethered amines, it is feasible to make a calculation of the approximate number of protonated amines at a certain pH from titration experiments of the **N3-S** solid in water. Following this procedure, we found percentages of protonation

(25) (a) Smith, R. M.; Martell, A. E. In *Critical Stability Constants*; Smith, R. M., Martell, A. E., Eds.; Plenum: New York, 1974−1989. (b) Martell, A. E.; Smith, R. M.; Motekaitis, R. M. NIST Critical Stability Constants of Metal Complexes Database, Texas A&M University, College Station, TX, 1993.

(26) Lloris, J. M.; Martínez-Máñez, R.; Perales, E.; Soto, J. *J. Chem. Res.* **1998**, 432−433.

of 44, 65, and nearly 100% for pH 6, 4, and 2, respectively. The titration experiments also show that there is a gradual protonation, as a function of the pH in agreement with the observed behavior, that shows a continuous change in "pore aperture" as a function of pH rather than an "on/off" behavior in a narrow pH rage.

We would also point out that some kind of interaction could also occur between certain polyamines and the silica surface. Although this would not be important on the external surface that is covered by the organosilane groups, certain electrostatic and hydrogen-bonding interactions might take place between certain polyamines and the surface of the pores close to the outside. However, be believe that this kind of interaction has a limited effect and thus it does not control the open/close action of the gate like-ensemble; i.e., an exclusive gate-like control via polyamine−silica interactions would be anion-independent. However, the anions play a remarkable role in dye delivery, as it will be shown below.

We were particularly concerned with the possibility that the observed effect was not caused by the amine-containing gate-like ensemble but was instead due to some simple interaction of the chloride anion or the proton concentration with the silica surface. To eliminate this possibility, $Ru(bipy)_3^{2+}$ delivery was repeated using an MCM-41 support loaded with the dye but not functionalized with the polyamines in the pore outlets. This solid displays no gate-like effect, and a very rapid pH-independent dye release is found in aqueous solution. Additional control experiments show that the gate-like outcome is only attainable using 3D supports, and a similar functional gating behavior could not be achieved based on functionalized "flat" 2D silica supports such as the solid **N3-SF**. This **N3-SF** solid, prepared from fumed silica (not including the mesoporous structure) and containing anchored polyamine groups and a certain amount of adsorbed $Ru(bipy)_3^{2+}$ dye, does not display any gate-like mechanism as a function of pH. Therefore, the pH-controllable gate-like functional effect is observed only for solids containing both nanoscopic pores and gate-like ensembles (tethered polyamines) at the pore outlets.

As stated above, the aperture of the gate might be related to the different pH-controlled conformation adopted by the tethered polyamines at the pore outlets. In order to study this effect in further detail, the pH-controlled modulation of the gate-like ensemble was studied by molecular dynamics simulations using force field methods. For this purpose a mesoporous silica structure was constructed, taking as base the plane $(1\bar{1}1)$ of the β-crystoballite structure on which large hexagonal nanopores were included, in order to simulate the mesoporous local surface structure. The calculations were carried out on a hexagonal unit cell that contains pores and wall thickness similar to those found in solids of the MCM-41 family. On this scaffold, the corresponding polyamines were anchored to the external surface. Because of the difficulty in finding the global energy minimum, molecular dynamics simulations were done to cover the most important parts of the potential energy surface using the thermal energy to escape from the local minima (see Experimental Section). Molecular dynamics simulations were applied for two opposing situations: (i) for non-protonated and (ii) for fully protonated amines. The results are shown in Figure 6, which plots a view parallel to the *z*-axis of the nanopore for the two cases. It can be seen how completely unprotonated amines

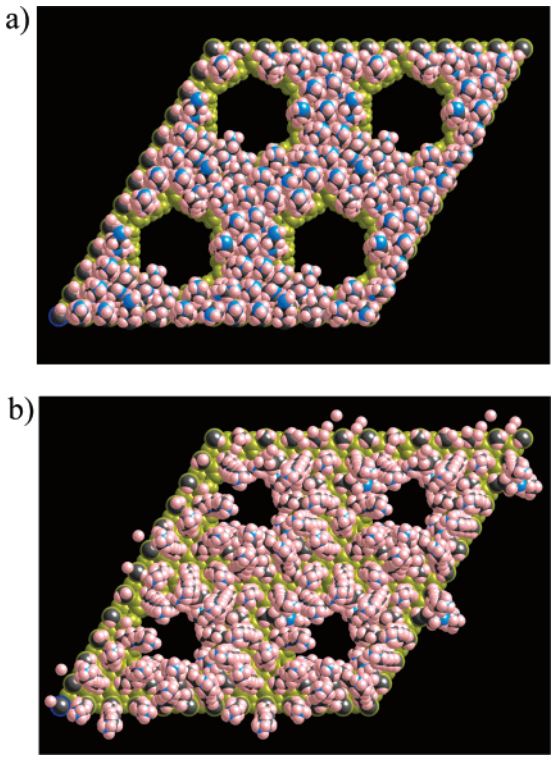

Figure 6. Perpendicular view of the axis of the nanopores for the (a) non-protonated and (b) fully protonated **N3-S** models. Blue, gray, and white are employed for nitrogen, carbon, and hydrogen atoms, respectively. The silica network (Si, O, and H) is represented in pale green.

Ⓦ A Quicktime video is available, showing the molecular dynamics simulation (0−5 ps) on the protonated **N3-S**. The plot shows the progress of energy (kilocalories) of the system as a function of the time (picoseconds).

display poor coverage of the pore, whereas completely protonated amines (simulating a pH 2 or lower) provide a clear reduction of the pore aperture. This latter phenomenon is clearly governed by the Coulomb repulsions between the ammonium groups that force the tethered polyamines to adopt a rigid-like conformation, just like a "hair-on-end skull" (Scheme 3, right). A molecular dynamics simulation on the protonated **N3-S** systems is available as a Quicktime video in the Web version of this article.[27]

Effect of the Size of the Gate-like Ensemble. The opening/closing functional effect would depend critically on whether the movable element (the gate-like ensemble) is able to effectively prevent the $Ru(bipy)_3^{2+}$ dye from exiting the pores. From Scheme 3, it is apparent that this function would depend on the size/length of the tethered polyamine. Hence, the anchoring in the pore outlets of amines of shorter structural dimensions should critically affect the delivery of the $Ru(bipy)_3^{2+}$ complex. To effect the controlled release of the ruthenium(II) dye, the hybrid solid **N1-S** was synthesized via functionalization of the MCM-41 scaffold with 3-aminopropyltrimethoxysilane. The **N1-S** system contains shorter tethered amines that form a smaller supramolecular gate-like ensemble on the external surface around the pores; i.e., the length of the appended polyamine decreases from 17 Å for **N3-S** to 9 Å for

(27) In the simulation, it can be observed how some of the anchored polyamines, such as those that are placed close to the pore outlets, are relaxed into the pore voids since hydrogen bonds with the oxygen atoms from the silica walls are formed. We believe this circumstance is favored due to the absence, in our theoretical models, of the $[Ru(bipy)_3]^{2+}$ guest in the pores but would be less important in the real experiments.

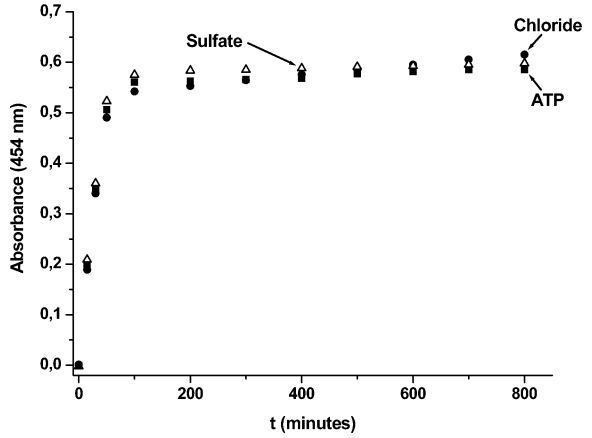

Figure 7. Dye release for solid **N1-S** in the presence of chloride, sulfate, and ATP anions ($C_{anion} = 1 \times 10^{-2}$ mol dm^{-3}) at pH 2.

N1-S. This significant change in size of the polyamine grafted onto the pore outlets dramatically affects the behavior of the molecular gate-like system. This can be observed in Figure 7, which shows the release profiles of the $Ru(bipy)_3^{2+}$ complex at pH 2.0 for the chloride, sulfate, and adenosine triphosphate (ATP) anions. This pH value was reached by acidification with hydrochloric acid, as described above, and the total concentration for chloride remained constant at 0.01 mol dm^{-3}. In spite of the presence of Coulombic repulsions between the ammonium groups and therefore the rigid conformation that the tethered amines in **N1-S** would adopt, their relatively short length makes them unable to block the pore openings, and the complete release of the ruthenium(II) complex was quickly achieved. Similar studies at pH 4 and 6 gave similar behavior; i.e., there was no appreciable gating effect.

Functional Anion-Controllable Gate-like Ensemble. The effectiveness of the gate-like ensemble, and therefore the delivery profile of the ruthenium(II) probe, is expected to depend on a number of factors. Apart from the pH-controllable function shown above, gate-like behavior is also expected at a certain pH derived from the interaction of the gate-like ensemble with certain anionic guests. This anion-controlled operational effect is based on the ability of polyamines to coordinate anions. Polyamines have thus been extensively explored as suitable groups for the design of synthetic receptors capable of binding selectively a number of inorganic and biologically important anionic guests.[28] In a first approximation, amine-containing receptors are polycations (polyammonium receptors) at neutral and acidic pH and bind anionic species via a combination of hydrogen bonding and Coulombic attraction. A more detailed look also reveals that protonated amines can serve as hydrogen donor elements, whereas non-protonated amines can act as hydrogen bond acceptors. The anchoring of the polyamines to the external surface of the MCM-41-based **N3-S** solid would additionally result in an improvement of their coordination ability, due to the occurrence of cooperative effects as a consequence of the presence of multiple amine/ammonium groups in the gate-like ensemble, which would enhance the electrostatic and hydrogen-bonding interactions with anionic species. In fact, recently reported systems of mesoporous MCM-41 supports functionalized with amines and anthracene as signaling unit have been used for the enhanced fluorimetric detection of certain anions in water based on the capacity of amine-containing material to coordinate anionic species.[29] In relation to the effectiveness of the gate, anion coordination on the amines tethered to the external surface of **N3-S** is expected to somehow modify the molecular topology of the gate-like ensemble near the pore outlets, especially when strong complexes would be formed, and therefore also expected to have a significant effect on the efficiency of the molecular gating open/close protocol.

A range of anions with different structural dimensions and charges, including chloride, sulfate, phosphate, and ATP ($C_{anion} = 1 \times 10^{-2}$ mol dm^{-3}), have been used to study the controlled release of the ruthenium(II) complex. The effect of these anions has been studied at different pH values, although for the sake of clarity only pH 2, 4, and 6 are discussed here. In all the cases, acidification was carried out with hydrochloric acid. The anion-controlled gating effect can clearly be seen in Figure 8. For instance, Figure 8a shows that, whereas the chloride anion is not able to completely hinder ruthenium(II) release, the sulfate and phosphate anions strongly inhibit dye delivery, and ATP completely closes the gate to the $[Ru(bipy)_3]^{2+}$ complex. This remarkable anion-controllable behavior can be explained in terms of formation of anion complexes with the tethered polyamines. For the correct interpretation of the interaction of certain guests (see below) with the gate-like ensemble, it is important to note that many anions display one or several stepwise protonations in water. Thus, anions that are conjugated bases of acids will accept protonation processes, and their charge will depend on their basicity constants. For instance, phosphate in water displays logarithm of stepwise protonation constants of 11.5, 7.7, and 2.1 for its first, second, and third protonations, respectively, whereas sulfate shows a logarithm for its first protonation of 1.9. Also, ATP displays stepwise protonation processes in water, with logarithms for the basicity constants of 6.8, 4.0, and 2.0. At pH 2, phosphate, sulfate, and ATP are mixtures of $H_2PO_4^-/H_3PO_4$, SO_4^{2-}/HSO_4^-, and H_2ATP^{2-}/H_3ATP^- species, respectively. Despite these considerations, in a first approach the observed pore blockage of the gate-like ensemble is somehow in agreement with the observed polyammonium−anion trend in water for complex formations that usually follow the order ATP ≫ phosphate ≥ sulfate ≫ chloride. A more detailed look at the polyammonium literature reveals that polyammonium receptors have been found to bind chloride very weakly. In relation to the gate-like ensemble, the interaction of the anchored polyammonium receptors with chloride would result in the formation of very weak and labile complexes that would not significantly modify the conformation of the gate-like ensemble at this pH. Also, when the anions chloride, sulfate,

(28) (a) Bianchi, A.; Micheloni, M.; Paoletti, P. *Inorg. Chim. Acta* **1988**, *151*, 269−272. (b) Král, V.; Andrievsky, A.; Sessler, J. L. *J. Chem. Soc., Chem. Commun.* **1995**, 2349−2350. (c) De Stefano, C.; Foti, C.; Gianguzza, A.; Giuffrè, O.; Sammartano, S. *J. Chem. Soc., Faraday Trans.* **1996**, *92*, 1511−1518. (d) Albelda, M. T.; Bernardo, M. A.; García-España, E.; Godino-Salido, M. L.; Luis, S. V.; Melo, M. J.; Pina, F.; Soriano, C. *J. Chem. Soc., Perkin Trans. 2* **1999**, 2545−2549. (e) Sancenón, F.; Benito, A.; Lloris, J. M.; Martínez-Máñez, R.; Pardo, T.; Soto, J. *Helv. Chim. Acta* **2002**, *85*, 1505−1516. (f) Albelda, M. T.; Aguilar, J.; Alves, S.; Aucejo, R.; Diaz, P.; Lodeiro, C.; Lima, J. C.; García-España, E.; Pina, F.; Soriano, C. *Helv. Chim. Acta* **2003**, *86*, 3118−3135. (g) Lloris, J. M.; Martínez-Máñez, R.; Padilla-Tosta, M.; Pardo, T.; Soto, J.; Tendero, M. J. L. *J. Chem. Soc., Dalton Trans.* **1998**, 3657−3662.

(29) (a) Descalzo, A. B.; Jiménez, D.; Marcos, M. D.; Martínez-Máñez, R.; Soto, J.; El Haskouri, J.; Guillém, C.; Beltrán, D.; Amorós, P. *Adv. Mater.* **2002**, *14*, 966−969. (b) Descalzo, A. B.; Marcos, M. D.; Martínez-Máñez, R.; Soto, J.; Beltrán, D.; Amorós, P. *J. Mater. Chem.* **2005**, *15*, 2721−2731.

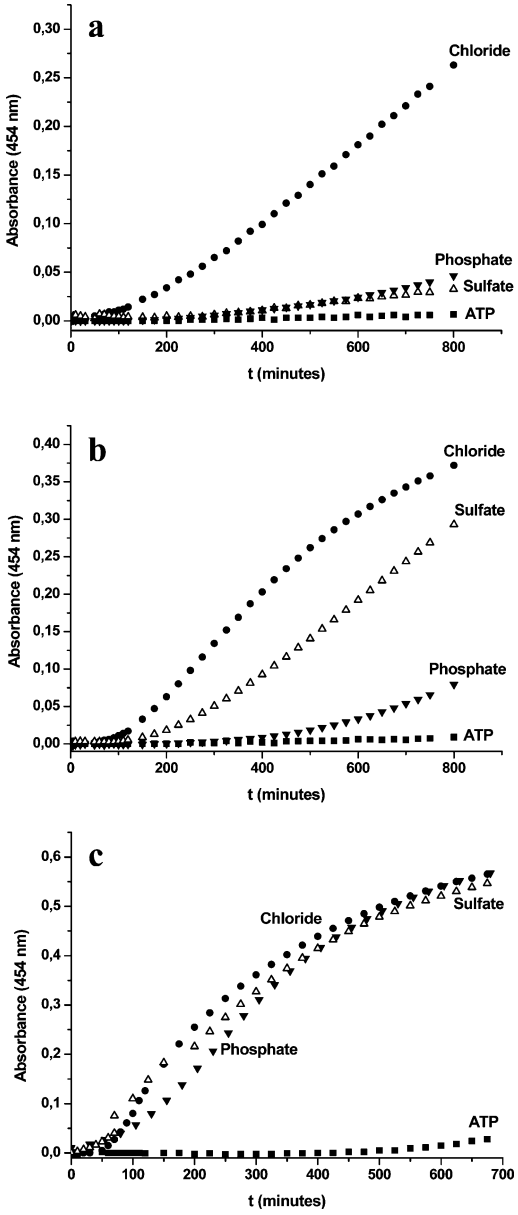

Figure 8. Dye release for solid **N3-S** in the presence of chloride, sulfate, phosphate, and ATP anions ($C_{anion} = 1 \times 10^{-2}$ mol dm^{-3}) at pH (a) 2, (b) 4, and (c) 6. In all cases, a lag time of around 100−150 s was observed and attributed to the time required to wet the solid.

and phosphate are compared side-by-side, it is apparent that those displaying stronger coordination with polyamines (i.e., phosphate via favorable hydrogen-bonding coordination (see below), or sulfate via stronger electrostatic interactions) are capable of inducing more effective closing of the polyamine-containing gate-like ensemble. The comparison between the behaviors found for phosphate and sulfate can be analyzed in more detail. From Figure 8, it is noticeable that, although at pH 2 sulfate is a more "charged" anion than phosphate, both anions appear to display a rather similar strong interaction with the gate-like polyammonium ensemble, in agreement with the analogous pore blockage exerted by both anions. Hence, as we will see below, it has been reported that the stability trends of phosphate complexes with polyamines are not strictly determined by electrostatic contributions, and the less charged phosphate species can form relatively strong stable complexes with polyammonium receptors.[30] This particular behavior of phosphate is related to the ability of the phosphate species to behave as acceptors and donors of hydrogen bonds, in contrast to SO_4^{2+} species, which can only act as hydrogen bond acceptors. Additionally, of all the anions studied, ATP is the largest one and the most "charged" and is able to form the strongest complexes, resulting in the complete pore blockage found in the presence of this anion.

For the anions ATP, sulfate, and phosphate, it is understood that, in addition to the gate-like superstructure formed at the pore outlets at a certain pH (the pH-dependent rigid-like conformation described above), there is a simultaneous cooperative effect created by the interaction of the protonated gate-like ensemble with anions. As these anions form considerably stronger complexes than chloride with polyammonium receptors, they are expected to form more rigid and bulkier polyammonium−anion gate-like structures that will more effectively inhibit the dye release. In short, the experimental results show that, at a certain pH, the gate-like superstructure is additionally and cooperatively more closed with increasingly stronger "gate-like ensemble"−"anion" interactions and bulkier anions.

The behavior of the gate-like ensemble in the presence of anions at pH 4 can be explained by following a similar analysis. At this pH, the amines are not as protonated as at pH 2, and therefore the interaction with anions would be weaker. Thus, at pH 4, ATP is the only key anion able to completely close the gate-like ensemble and avoid dye liberation. The delivery rate for other anions follows the order $Cl^- > SO_4^{2-} \gg H_2PO_4^-$. At the neutral pH of 6, the polyamines are less protonated, the interactions of the **N3-S** solid with these anions are drastically reduced, and all the anions except ATP show similar delivery kinetics; i.e., basically the gate is open in the presence of chloride, sulfate, and phosphate and completely closed for ATP. This remarkably selective behavior of ATP is most likely related to the well-known ability of ATP to strongly coordinate polyamines, even at neutral and basic pH. It is noticeable that certain anions, such as ATP, act as molecular taps in relation to the **N3-S** solid and are able to completely inhibit the delivery of the enclosed ruthenium(II) complex.

We were also concerned with the possibility that the anion-induced effect could be due to some simple differences in the adsorption affinity of the different anions to the silica surface at a certain pH. To eliminate this possibility, the $Ru(bipy)_3^{2+}$ delivery was repeated at pH 6 and pH 2 in the presence of ATP ($C_{ATP} = 0.01$ mol dm^{-3}) but using an MCM-41 support loaded with the dye but not functionalized with the polyamines in the pore outlets. ATP was chosen because it is the anion that induces in **N3-S** a complete pore blockage (see Figure 8). The experiments showed that this solid displays no gate-like effect, and the $Ru(bipy)_3^{2+}$ is released immediately in aqueous solution at both pH 6 and pH 2 in the presence of the ATP anion. These control experiments stress the interpretation that the gate-like system is controlled by the supramoleclar interaction of the anions with the tethered polyamines as explained above and is not due to simple anion interactions with the silica surface.

(30) (a) Beer, P. D.; Cadman, J.; Lloris, J. M.; Martínez-Máñez, R.; Padilla-Tosta, M. E.; Pardo, T.; Smith, D. K.; Soto, J. *J. Chem. Soc., Dalton Trans.* **1999**, 127−133. (b) Lloris, J. M.; Martínez-Máñez, R.; Padilla-Tosta, M. E.; Pardo, T.; Soto, J.; García-España, E.; Ramírez, J. A.; Burguete, M. I.; Luis, S. V.; Sinn, E. *J. Chem. Soc., Dalton Trans.* **1999**, 1779−1784. (c) Lloris, J. M.; Martínez-Máñez, R.; Padilla-Tosta, M. E.; Pardo, T.; Soto, J. *Helv. Chim. Acta* **1999**, *82*, 1445−1453.

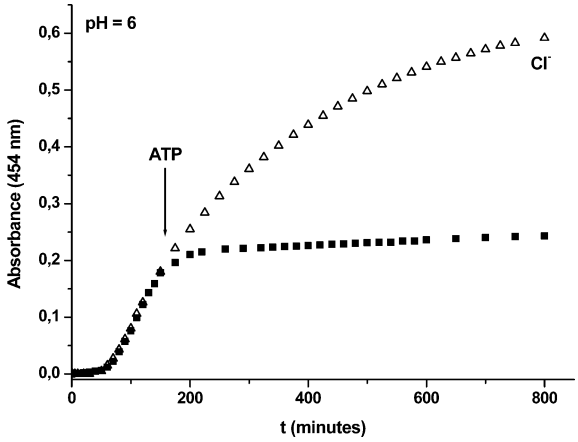

Figure 9. Dye release for solid **N3-S** in the presence of chloride anions ($C_{chloride} = 1 \times 10^{-2}$ mol dm^{-3}) at pH 6 until $t = 170$ min (indicated by the arrow), when ATP ($C_{ATP} = 1 \times 10^{-2}$ mol dm^{-3}) was added to the solution.

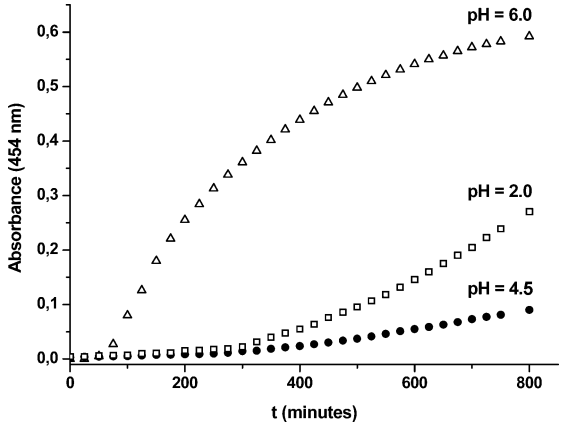

Figure 10. Dye release for solid **N3-S** in the presence of isobutyrate anion at pH 2, 4, and 6.

In order to further explore the versatility in the control of the pore aperture using simple external stimuli, the release profile was monitored at pH 7 in the presence of chloride (gate open), and the delivery conditions were changed at a certain time by adding ATP to the solution (without changing the pH). The effect observed is shown in Figure 9. The presence of ATP induced an immediate and complete blockage of the pore. Changes in the pH can also be used to easily control the pore aperture. Thus, for instance, the closed gate-like ensemble at pH 2 in the presence of phosphate that inhibits dye release can be readily opened by changing the pH to 7 (not shown). These experiments demonstrate the possibility of straightforwardly controlling the pore aperture in water of gate-like ensembles using simple external stimuli (pH or presence of certain anions).

In conclusion, both pH-controlled and anion-controlled gate-like effects occur in solid **N3-S**. Apart from the pH-controlled "open/close" effect arising from hydrogen-bonding interactions between amines (open gate) and electrostatic repulsions between polyammonium groups (closed gate), a synergic anion-controlled outcome results from the interaction (formation of complexes) between the protonated amines and certain anions. As can be seen from the data above, the choice of certain anionic guests results in different behaviors of the gate-like ensemble of the **N3-S** material, from basically no action (chloride) to complete (ATP) or partial pore blockage, depending on the pH (sulfate and phosphate). Figure 8 shows how, in all the cases studied (except for ATP, which closes the gate throughout the pH range), there is gradual pore blockage when moving from neutral to acidic pH as a consequence of the gradual protonation of the amines and the synergic interaction with charged anions.

At this point, we were also interested in demonstrating that the gate-like ensemble containing amines is highly adaptable and takes advantage of the well-known versatile chemistry of the polyamines as anion receptors in aqueous solution. As has been stated above, it is well-known that the strength of the interaction of anions with a certain polyamine can be controlled not only by the pH, which modulates the relative number of amine/ammonium groups in the receptor, but also by the acid−base behavior of the guest. Application of this idea for the modulation of the gating behavior of the gate-like ensemble is illustrated by the dye release from the pores of solid **N3-S** at pH 2, 4.5, and 6 in the presence of isobutyrate ($(CH_3)_2CH-COO^-$, see Figure 10). This is a relatively large anion, with a pK_a of 4.8. As we have seen before, at pH 6, the amines are only partially protonated, and the interaction of **N3-S** with the anion $(CH_3)_2CH-COO^-$ is not able to close the gate; delivery profiles similar to those found for chloride, sulfate, and phosphate are observed. At pH 4.5, there is a mixture of $(CH_3)_2CH-COO^-$ and $(CH_3)_2CH-COOH$ species that is able to partially close the gate via electrostatic and hydrogen-bonding interactions with the partially protonated polyamines. However, upon acidification with hydrochloric acid to pH 2, the isobutyrate anion is protonated, there is no interaction between the polyammonium groups and the isobutyric acid, and the gate opens partially (i.e., a response similar to that found for the gate at pH 2 in the presence of chloride is found; see Figure 5).

In order to go deeper into the factors that control the gate-like ensemble, the influence of the presence of anions on the gating effect has also been studied by molecular dynamics simulations. This was carried out on **N3-S** containing fully protonated amines (simulating pH 2 or lower), using a model similar to that shown above but including in the simulation the corresponding amount of the anion in order to compensate for the charge of the protonated ammonium groups. For this computational study, the anions fluoride, chloride, iodide, and dihydrogen phosphate were selected. Iodide and fluoride anions were not studied in real solutions (see above) because the former can be partially transformed into tri-iodide and the latter would attack the silica matrix at acidic pH, giving imprecise experimental results. However, they were used in the molecular dynamics simulations because they are ideal anionic systems, together with chloride and dihydrogen phosphate, having the same charge but different sizes. Calculations using the universal force field (UFF) were performed on the whole system to reach the fully relaxed geometry. From these final configurations, we were interested in a first approach to examine the effect of the anions on the conformation of the gate-like ensemble (the tethered protonated polyamines). To observe this effect, the pore size was calculated in the fully relaxed geometry by "removing" the corresponding anions to take into account only the conformation of the anchored protonated polyamines. An estimation of the average pore openings of the gate-like ensemble in the presence of different anions (but not considering the anions for the pore size calculations) is shown in Table 2.

Generally, the simulations show that these anions, due to their negative charge, tend to be placed between the protonated

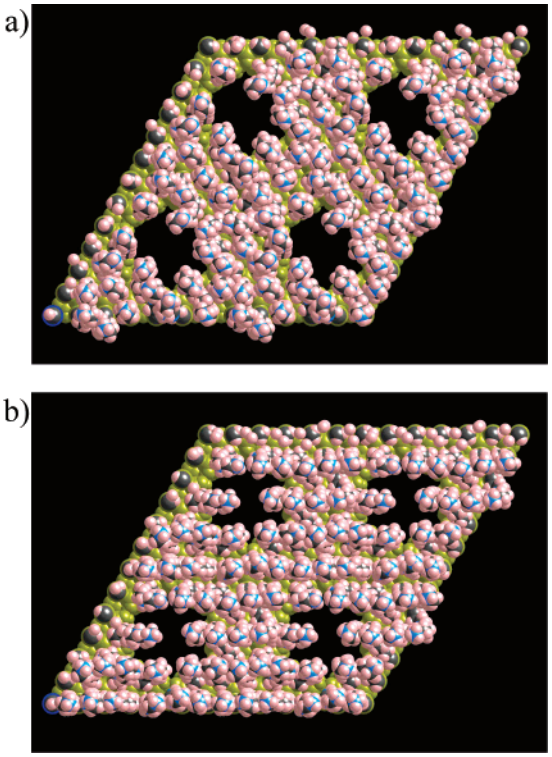

Figure 11. Perpendicular view of the axis of the nanopores for the fully protonated **N3-S** system in the presence of (a) fluoride and (b) iodide. The graphic representation shows only the conformation of the polyamines and does not show the position of the anions. Blue, gray, and white are employed for nitrogen, carbon, and hydrogen atoms, respectively. The silica network (Si, O, and H) is represented in pale green.

Table 2. Nanopore Diameter, *d* (in Å), Calculated from the Molecular Dynamic Simulations for the Non-protonated and Protonated Models (Some Models Include the Presence of Different Anions)

model/anion[a]	*d* (Å)	anion volume (Å^3)[c]
N3-S(p)	6.8	
N3-S(p)/F^-	7.0[b]	9.9
N3-S(p)/Cl^-	6.6[b]	24.8
N3-S(p)/I^-	5.0[b]	44.6
N3-S(p)/$H_2PO_4^-$	4.5[b]	56.5

[a] The label (p) is used to stress that the polyamines are protonated. [b] The pore size is calculated taking into account only the polyamine conformation and "removing" the corresponding anion from the final relaxed geometry. [c] Anion volume from the literature: Marcus, Y.; Jenkins, H. D. B.; Glasser, L. *J. Chem. Soc., Dalton Trans.* **2002**, 3795. The anion volume for phosphate is that for the species PO_4^{3-}.

polyamines, creating a shielding effect between the charged ammonium groups. In the model, larger anions push the tethered polyamines to the pore openings more efficiently, and therefore the pore aperture is reduced; i.e., pore apertures of 7.0, 6.6, 5.0, and 4.5 Å are observed for F^-, Cl^-, I^-, and $H_2PO_4^-$, respectively. As a representative example, Figure 11 shows the conformation of the gate-like ensemble calculated in the presence of fluoride and iodide anions.

It is also noticeable that the gate-like ensemble shows a slightly larger pore size (7.0 Å) in the presence of the fluoride anion than that observed when anions are not included in the model (6.8 Å). The small size of the fluoride anion results in a more compact arrangement of the polyamines. A representation of this anion effect is shown in Scheme 4.

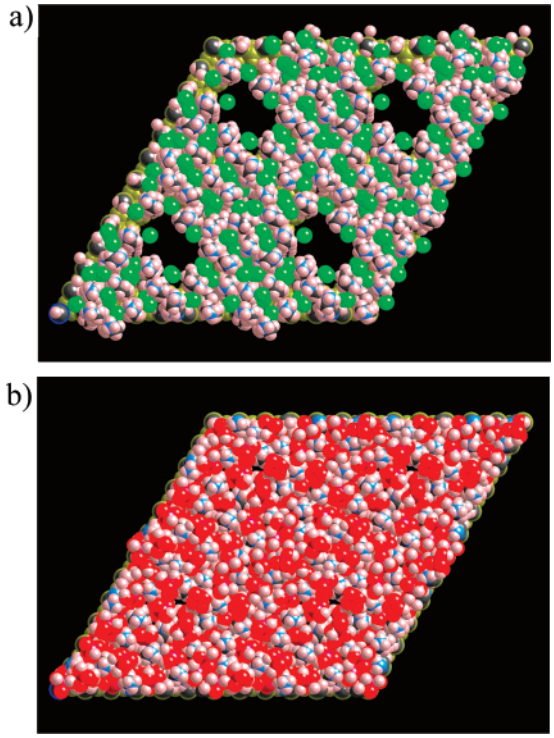

Figure 12. Perpendicular view of the axis of the nanopores for the fully protonated **N3-S** system in the presence of (a) chloride and (b) dihydrogen phosphate. Blue, gray, and white are employed for nitrogen, carbon, and hydrogen atoms, respectively. The silica network (Si, O, and H) is represented in pale green. The chloride is represented in green, whereas the phosphorus and oxygen atoms from the phosphate groups are represented in red.

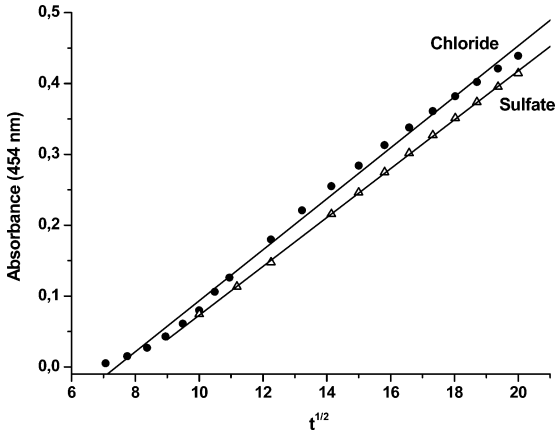

Figure 13. Delivery rate of the ruthenium(II) complex from the pores of solid **N3-S** at pH 6. The delivery is a diffusive process, as suggested by the linear relationship of the experimental absorbance at 454 nm (dye delivered) and the square root of the time (*t*) for the delivery of ruthenium(II) complex from the pores of solid **N3-S** at pH 6 in the presence of chloride and sulfate anions.

In addition to these calculations, it should also be remembered that the real pore aperture is a combination of the conformation of the gate-like ensemble and the presence of the corresponding anion. Thus, if we take into account the effective presence of the corresponding anions, a further pore-blockage effect that is related to anion size and the possibility of forming hydrogen-bonding networks can be clearly observed. This final upshot is shown in Figure 12, which pictures a parallel view of the nanopore for the protonated **N3-S**(p) system in the presence of chloride and dihydrogen phosphate. Whereas in the former a

Scheme 4. Schematic Representation of the Molecular Gate in the Absence (b) and in the Presence of Small (c) and Big (a) Anions[a]

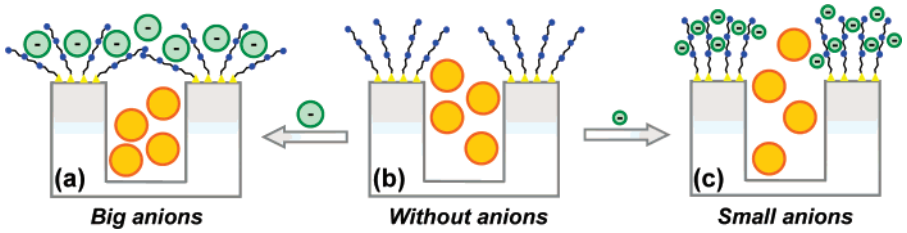

[a] The anions and dye are displayed in green and yellow, respectively.

neat pore is observed, for the latter the formation of a dense hydrogen bond network together with the anion itself and the polyamines (gate ensemble) results in complete coverage of the nanopore, in agreement with the non-release of the $[Ru(bipy)_3]^{2+}$ complex found experimentally, as observed in Figure 8a.

Molecular "Gates" versus Molecular "Valves". Selectivity patterns can now be discussed in terms of kinetic rates of liberation of $Ru(bipy)_3^{2+}$ dye from the amine-functionalized dye-containing material **N3-S**. The delivery of the rutheniun(II) complex to the solution in a molecular gate-like system was first analyzed considering that a simple diffusion process occurs. This can only be applied when the gate-like ensemble does not exert any asymmetric, kinetic, or thermodynamic constraint on the delivery process. In fact, the term "diffusion" implies that the process should be essentially reversible. Based on this diffusion concept, the kinetics of molecular release from pore voids of the mesoporous **N3-S** material could be explained using the Higuchi model.[31] According to this model, the release of the ruthenium(II) complex can be described as a square root of a time-dependent process based on Fickian diffusion. The amount of guest release, Q_t, per unit of exposed area at time t can then be described by the simple relation

$$Q_t = k_H\sqrt{t} \tag{1}$$

where k_H is the release rate constant for the Higuchi model. When the dye is dispersed inside the matrix and diffusion occurs through solvent-filled pores, the formulation of the constant is where D is the diffusivity of the dye in the solvent, τ is the

$$k_H = f(D, \epsilon, \tau, C, A) \tag{2}$$

tortuosity factor of the system, ϵ is the porosity of the matrix, A is the total amount of dye present in the matrix, and C is the solubility of the guest in the solvent used. This equation has generally been satisfactorily applied for related porous silica (not containing gate-like ensembles) used for the no controlled release of drugs.[32]

The delivery of the ruthenium(II) complex from the pores of solid **N3-S** at pH 6 is basically a diffusive process. Equation 1 provides an explanation of the delivery of ruthenium(II) dye at pH 6 in the presence of chloride, sulfate, and phosphate anions. Figure 13 shows the Higuchi square root of the time plot for the release of the ruthenium(II) dye in the presence of chloride and sulfate anions. Good linearity is found until $t \approx 400$ min, after which a deviation from the overall linearity was observed (not shown). This effect (two or more steps in the release profiles) has also been described in other no controlled kinetic release studies of certain guests (usually drugs) from porous carrier materials. As we have seen before, at pH 6, the gate-like ensemble is open in the presence of these anions, and in all cases similar release rate constants (k_H) were observed; i.e., 3.64×10^{-2}, 3.65×10^{-2}, and 3.64×10^{-2} for chloride, sulfate, and phosphate, respectively, using eq 1. From a molecular point of view, it can be concluded that, at this pH, the tethered amines behave like loose threads that basically allow bidirectional and diffusive mass transport. For certain anions, such as ATP, which form very strong complexes, the tortuosity factor τ is too high, and there is no appreciable dye delivery. The ATP anion acts as a molecular cork or tap that completely inhibits delivery from the pore voids.

In a first approach, we also applied the Higuchi model for the evaluation of the delivery kinetics at pH 4 and 2. However, it was not possible to fit the experimental data with this diffusive equation, and it became apparent that the experimental points deviate significantly from the expected linear plot of a square root of a time-dependent process. A possible explanation of why the dye release does not obey a diffusive model at acidic pH might be related to the conformation of the gate-like ensemble and the additional rigidity imposed by the synergic interaction with anions, which is expected to result in an asymmetric constraint in relation to the molecular mobility of the dye through the pore. From the nanoscopic topology of the gate-like ensemble (see, for instance, Scheme 3), it is apparent that, for a certain molecule, it would be easier to leave than to enter the pores from the bulk solution. Thus, whereas at pH 6 the cooperative effect of the loose filament in the pore outlets makes the gate-like ensemble act as a simple pore (except for ATP), at acidic pH the nanoscopic structure of rigid filaments would basically act as a molecular "valve", inhibiting access to the inner pores but allowing mass transport from the pores to the bulk solution.

We developed a model (eq 3) for the interpretation of the experimental data of dye delivery for the **N3-S** solid at pH 4 and 2, based on the idea that the rate of release of the guest in the pores is proportional only to the fraction of the space occupied by the dye in the pore voids. The formalism that leads

$$\frac{n_0}{V}\log\left(1 + \frac{V}{n_0}[A]\right) = k(t - t_0) \tag{3}$$

to the deduction of this equation is given in the Experimental Section. In this relation, k is the release rate constant in this model, t_0 is the lag time for the activation of the release process, n_0 is the maximum number of moles of dye that can be loaded

(31) (a) Higuchi, T. *J. Pharm. Sci*. **1961**, *50*, 874. (b) Higuchi, T. *J. Pharm. Sci*. **1963**, *52*, 1145.
(32) See, for instance: (a) Vallet-Regi, M.; Rámila, A.; del Real, R. P.; Pérez-Pariente, J. *Chem. Mater*. **2001**, *13*, 308. (b) Muñoz, B.; Rámila, A.; Pérez-Pariente, J.; Díaz, I.; Vallet-Regi, M. *Chem. Mater*. **2003**, *15*, 500. (c) Anderson, J.; Rosenholm, J.; Areva, S.; Lindén, M. *Chem. Mater*. **2004**, *16*, 4160.

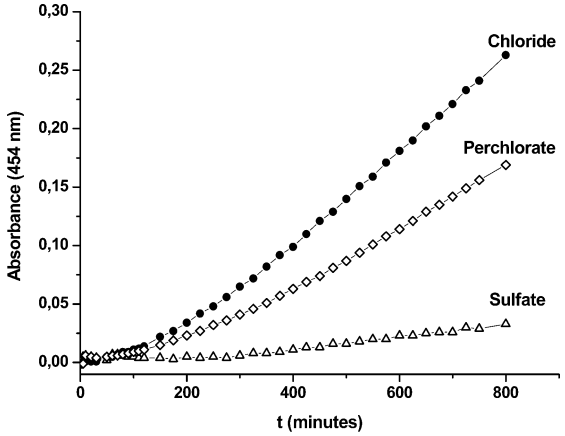

Figure 14. Plot of the experimental absorbance at 454 nm versus time and the adjusted curve (solid line), using eq 3, for the delivery of ruthenium(II) complex from the pores of solid **N3-S** at pH 2 in the presence of chloride, perchlorate, and sulfate anions.

Table 3. Release Rate (k) for the Ruthenium(II) Dye Delivery from the Pores of the **N3-S** Solid at pH 4 and 2 in the Presence of Certain Anions

	$k \times 10^{-8}$		
anion	pH 2	pH 4	anion volume (Å^3)[a]
chloride	1.12	1.90	24.8
perchlorate	0.75	1.51	57.9
sulfate	0.16	1.36	51.0
phosphate	0.17	0.30	56.5
ATP	*b*	*b*	

[a] Anion volume from the literature: Marcus, Y.; Jenkins, H. D. B.; Glasser, L. *J. Chem. Soc., Dalton Trans.* **2002**, 3795. The anion volumes for sulfate and phosphate are those for the species SO_4^{2-} and PO_4^{3-}. [b] No dye delivery was observed in the presence of ATP.

in the pores (for 10 mg of solid, this is ca. 1.7×10^{-6} mol), V is the the volume of the solution (0.025 dm^{-3}), and [A] is the concentration (in mol dm^{-3}) of the ruthenium(II) complex in the solution at time t. For these particular pH values, delivery in the presence of the perchlorate anion was also studied. Figure 14 shows a plot of the experimental absorbance at 454 nm versus time and the adjusted curve (solid line), using eq 3, for chloride, sulfate, and perchlorate anions at pH 2.

The values obtained for the dye delivery release rate (k) of the **N3-S** solid at pH 4 and 2 in the presence of certain anions are shown in Table 3. The model is valid for the study of the release kinetics of ruthenium(II) dye in the **N3-S** solid at acidic pH, but not at pH 6 (eq 3 does not fit the experimental values at neutral pH). The different k values obtained for different anions is somehow related to the different activation energy required for ruthenium(II) dye in passing through the molecular valve.

The calculation of k values through the use of eq 3 gives in-depth information on the factors that control the opening/closing protocol of the gate-like ensemble. Figure 15 shows a plot of the dye release kinetic constants for the chloride, perchlorate, sulfate, and phosphate anions at pH 2 and 4 as a function of the product (anion charge) × (anion volume). A fairly good linear correlation is found for both pH values for the chloride, perchlorate, and sulfate anions, strongly suggesting that the main driving forces in the closing of the gate-like ensemble are (i) the electrostatic anion−polyammonium interaction and (ii) the volume of the anionic species. Remarkably,

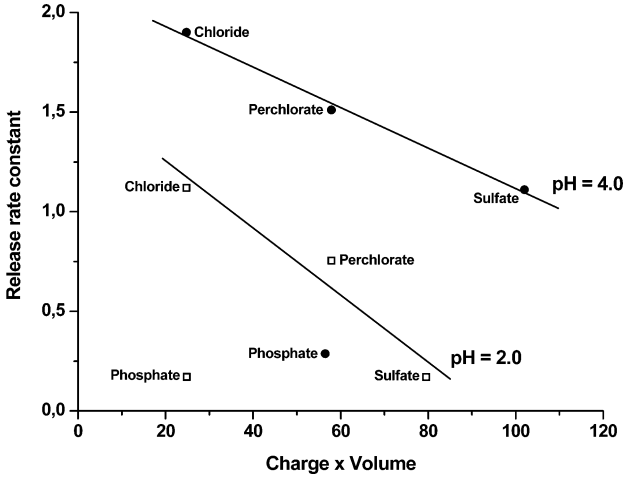

Figure 15. Plot of the release kinetic constants (k) for chloride, perchlorate, sulfate, and phosphate anions at pH 2 and 4 as a function of the product (anion charge) × (anion volume). For pH vales where more than one anionic species are found, the anion charge refers to the average charge, calculated as $\sum X_i q_i$ (where X_i and q_i are the molar fraction and charge of species i, respectively).

this trend is not followed by phosphate, which displays a much stronger gate-closing ability than that expected for simple charge−charge polyammonium−phosphate attractive forces, indicating the importance of the hydrogen-bonding interactions exerted by this anion when forming complexes with amine/ammonium receptors (vide ante).

Conclusions

Although some hybrid supramolecular functions are still in their infancy, we believe that a very promising research area has arisen from the blending of the chemistry of nanoscopic solid materials with supramolecular concepts. In particular, we have demostrated that it is possible to carry out traditional coordination chemistry on surfaces (3D surfaces) that result in enhanced functional supramolecular aspects such as the development of nanoscopic gate-like ensembles. Specifically, we have established that, when using linear polyamines anchored to mesoporous materials, both pH-controlled and anion-controlled gate-like effects could occur in pure water. The pH-controlled "open/close" mechanism arises most likely from hydrogen-bonding interactions between amines (open-gate) and Coulombic repulsion between ammonium groups (closed-gate). Additionally, a synergic anion-controlled outcome would result from the interaction (formation of complexes) between the protonated amines and a certain anion. The experimental observations have been confirmed by means of a theoretical study based on molecular dynamics using force field methods. We believe that these and other similar studies on solids can help in the development of new functional nanogates in water by using well-known supramolecular and coordination tools.

Experimental Section

Synthesis. (a) General Methods. XRD, TGA, IR spectroscopy, elemental analysis, EDX microscopy, N_2 adsorption−desorption, and UV−visible spectroscopy techniques were employed to characterize the materials obtained. X-ray measurements were performed on a Seifert 3000TT diffractometer using Cu Kα radiation. Thermogravimetric analyses were carried out on a TGA/SDTA 851e Mettler Toledo balance, using an oxidant atmosphere (air, 80 mL/min) with a heating program consisting of a ramp of 10 °C/min from 393 to 1273 K. IR

spectra were recorded on a Jasco FT/IR-460 Plus instrument between 400 and 4000 cm^{-1}, diluting the solids in KBr pellets. EDX analyses were performed on a Jeol JSM 6300 instrument operated at 20kV. N_2 adsorption−desorption isotherms were recorded on a Micromeritics ASAP2010 automated sorption analyzer. The samples were degassed at 120 °C in a vacuum overnight. The specific surface areas were calculated from the adsorption data in the low-pressure range using the BET model. Pore size was determined following the BJH method. UV−visible spectroscopy was carried out with a Lambda 35 UV/vis spectrometer (Perkin-Elmer Instruments).

For the synthesis of ordered mesoporous materials, tetraethyl orthosilicate (TEOS), *n*-cetyltrimethylammonium bromide (CTAB), sodium hydroxide (NaOH), and triethanolamine ($TEAH_3$) were purchased from Aldrich. The organosiloxane derivatives 3-[2-(2-aminoethylamino)ethylamino]propyl-trimethoxysilane and 3-aminopropyltriethoxysilane, for the synthesis of the solids **N3-S** and **N1-S**, respectively, and the dye tris(2,2′-bipyridyl)ruthenium(II) chloride hexahydrate ($Ru(bipy)_3Cl_2 \cdot 6H_2O$) were provided by Aldrich. Nonporous amorphous fumed silica with a surface area of ca. 200 m^2/g was provided by Aldrich. It was used with 3-[2-(2-aminoethylamino)ethylamino]propyl-trimethoxysilane for the synthesis of the solid **N3-SF**. For the anion-controlled gate-like studies, the following salts were used: adenosine-5′-triphosphate disodium salt hydrate 99% (ATP), sodium chloride (NaCl), sodium sulfate (Na_2SO_4), and sodium phosphate dodecahydrate ($Na_3PO_4 \cdot 12H_2O$). All the reactants were used as received from Sigma-Aldrich.

(b) Synthesis of MCM-41. The synthesis strategy we used to prepare MCM-41 silicas is an application of the so-called "atrane route", a simple preparative technique based on the use of triethanolamine-related ($TEAH_3$) ligands (in general "atranes", and "silatranes" for the silicon-containing complexes) as hydrolytic inorganic precursors and surfactants as porogen species. The molar ratio of the reagents in the mother liquor was fixed to 8 $TEAH_3$:2 TEOS:0.52 CTAB:0.5 NaOH:180 H_2O for the synthesis of MCM-41. In a typical synthesis leading to the MCM-41 pure silica, 4.23 g of CTAB was added at 60 °C to a solution of $TEAH_3$ (23 mL) containing 0.045 mol of a silatrane derivative (e.g., in the form of $Si(TEA)(TEAH_2)$, TEA is the fully deprotonated ligand). Next, 180 mL of water was slowly added with vigorous stirring at 50 °C. After a few minutes, a white suspension was formed. This mixture was aged at room temperature overnight. The resulting powder was collected by filtration and washed with water and ethanol. Finally, the solid was dried at 70 °C. To prepare the final porous material, the as-synthesized solid was calcined at 550 °C using oxidant atmosphere for 5 h in order to remove the template phase. Finally, 1 g of calcined MCM-41 was suspended in 100 mL of 1 M HCl in ethanol; the mixture was stirred and refluxed for 4 h. After the process of rehydroxylation by acid hydrolysis, the resulting solid was filtered, washed with water until the pH reached 5−6, and dried at 70 °C for 12 h. The calcination process promotes the condensation of unreacted silanol groups, and the last step was performed in order to minimize loss of surface silanols. The presence of pores of uniform size lined with silanol groups makes these materials potentially interesting as hosts for a variety of guest chemical species.

(c) Synthesis of N3-S. In a typical synthesis, 1.00 g of activated MCM-41 and 0.6 g (0.8 mmol) of tris(2,2′-bipyridyl)ruthenium(II) chloride hexahydrate were suspended in 50 mL of anhydrous acetonitrile inside a round-bottom flask connected to a Dean−Stark (trap) apparatus in an inert atmosphere. The suspension was refluxed (110 °C) in azeotropic distillation, collecting 20 mL in the trap in order to remove the adsorbed water. The mixture was stirred for 24 h at room temperature with the aim of achieving maximum loading in the pores of the MCM-41 scaffolding. A small fraction of the suspension was extracted to obtain a solid that could be used as "blank material" (dye-loaded solid but without external amine functionalization) for comparison purposes. Afterward, an excess of 3-[2-(2-aminoethylamino)-ethylamino]propyl-trimethoxysilane (4.3 mL, 15.0 mmol) was added, and the suspension was stirred for 5.5 h. Finally, the orange solid (**N3-S**) was filtered off, washed with 30 mL of CH_3CN, and dried at 70 °C for 12 h. Following this post-synthesis grafting method, the anchored polyamines should be preferentially attached to the pore outlets. The functionalization would take place more easily on the external surface than inside the channels, which are filled with the $Ru(bipy)_3^{2+}$ cation dye.

(d) Synthesis of N1-S. The same procedure described above was followed, but in this case, 3.5 mL (15 mmol) of 3-(aminopropyl)-triethoxysilane was used as the surface functionalization reactant.

(e) Synthesis of N3-SF. In a typical synthesis, 1.00 g of activated fumed silica and 0.6 g (0.8 mmol) of tris(2,2′-bipyridyl)ruthenium(II) chloride hexahydrate were suspended in 50 mL of anhydrous acetonitrile inside a round-bottom flask connected to a Dean−Stark (trap) apparatus in an inert atmosphere. The suspension was refluxed (110 °C) in azeotropic distillation, collecting 20 mL in the trap in order to remove the adsorbed water. The mixture was stirred for 24 h at room temperature. Afterward, an excess of 3-[2-(2-aminoethylamino)ethylamino]propyl-trimethoxysilane (4.3 mL, 15.0 mmol) was added, and the suspension was stirred for 5.5 h. Finally, the orange solid (**N3-SF**) was filtered off, washed with 30 mL of CH_3CN, and dried at 70 °C for 12 h.

Dye Release Studies. Twenty-five-milliliter portions of aqueous solutions containing the corresponding anion ($C_{anion} = 1 \times 10^{-2}$ mol dm^{-3}) at different pH values were used for evaluating the gate-like effect by studying dye release from the pore voids of the amine-functionalized materials. A cartridge loaded with 10 mg of the corresponding solid (**N3-S**, **N1-S**, **N3-SF**, and related blanks) was inserted into a flux cell, and the system was then filled with the corresponding solution (water at a certain pH) and maintained in circulation for 800 min. The delivery of the $[Ru(bipy)_3]^{2+}$ dye from the pore voids to the aqueous solution was monitorized via the spin-allowed d−π metal-to-ligand charge-transfer transition band of the $[Ru(bipy)_3]^{2+}$ dye centered at 454 nm.

Model of the Release of the Guest. The model for the delivery of ruthenium(II) from the pore voids of the **N3-S** at acidic pH is based on the concept that the rate of release of the guest in the pores is proportional to the fraction of the occupied space in the pore voids:

$$v = k\Theta$$

where Θ is the fraction of the number of moles of the guest in the pores at a certain time, *n*, and the maximum number of guests that can be loaded in the pores, n_0 (for 10 mg of solid, this is 1.7×10^{-6} mol). We can then write

$$\Theta = \frac{n}{n_0} = \frac{n_0 - n_A}{n_0} = 1 - \frac{n_A}{n_0}$$

where n_A is the number of moles of guest released into the solution at that specific moment. Bearing in mind that

$$n_A = V[A]$$

where *V* is the volume of the solution (usually 0.025 dm^{-3}) and [A] is the concentration (in mol dm^{-3}) of the guest at time *t*, the kinetic equation is

$$\frac{d[A]}{dt} = k\left(1 - \frac{V}{n_0}[A]\right) \quad (4)$$

which, by integration, results in eq 3 as described in the Results and Discussion:

$$\frac{n_0}{V}\log\left(1 + \frac{V}{n_0}[A]\right) = k(t - t_0)$$

Computational Details. Three requirements must be met by the silica crystal structure chosen to build a suitable two-dimensional model of a mesoporous silica of the **MCM-41** family: (i) one of the surfaces must present only terminal oxygen atoms, (ii) the opposite surface should show only terminal silicon atoms that will act as anchoring points of the polyamine, and (iii) the morphology of the mesopore must be close to an ideal cylindrical geometry. In accordance with these conditions, we selected the crystal structure of β-crystoballite. Cleavage of the crystal structure parallel to the $(1\bar{1}1)$ plane allowed us to obtain a mesoporous model with large hexagonal nanopores. This model can be described as a hexagonal supercell with the following parameters: $a = b = 30.377$ Å, $\alpha = \beta = 90.0°$, and $\gamma = 120.0°$. The size of this "supercell" was chosen in order to generate pores and walls with dimensions similar to those experimentally found in the **MCM-41** family of solids. The depth of the pores in this two-dimensional model is 28.7 Å. The terminal oxygen atoms in the surfaces and inside the nanopore were protonated. The polyamines were anchored to the terminal silicon atoms placed on the surface.

Due to the huge size of the models needed for this kind of study, the calculations were carried out using force field methods. For this purpose, the universal force field (UFF) suggested by Rappe et al. was employed.[33] In order to find the global energy minimum, because of the presence of many local minima, molecular dynamics simulations were done to cover the most important parts of the potential energy surface, using the thermal energy to overcome the local minima. These molecular dynamics simulations were carried out within the canonical ensemble (number of particles, volume, and temperature are constant) for a time of 50 ps with a time step of 1 fs. Among the conformations observed during the molecular dynamics simulation, the most stable geometry was taken as the starting point for a later geometry optimization. The geometry optimizations and molecular dynamics simulations were performed with the Cerius2 package.[34] In the evaluation of the nanopore diameter (Table 3), the anions placed inside the pore were not considered, due to their considerable mobility.

Acknowledgment. The authors wish to express their gratitude to the Ministerio de Ciencia y Tecnología (projects CTQ2006-15456-C04-01, MAT2005-01355, and CTQ2005-08123-C02-02/BQU), Generalitat Valenciana (project GV06/101), and the Catalan Government (grant 2005SGR-00036) for financial support.

JA0756772

(33) (a) Rappe, A. K.; Casewith, C. J.; Colwell, K. S.; Goddard, W. A., III; Skiff, W. M. *J. Am. Chem. Soc.* **1992**, *114*, 10024−10035. (b) Castonguay, L. A.; Rappe, A. K. *J. Am. Chem. Soc*. **1992**, *114*, 5832−5842. (c) Rappe, A. K.; Colwell, K. S. *Inorg. Chem.* **1993**, *32*, 3438−3450.

(34) *Cerius2*, version 3.8; Molecular Simulations Inc.: San Diego, CA, 1998.